Nonlinear Dynamic Aeroelasticity Response Analyses of Very Flexible Aircraft at Conceptual Design Stage: A Sensitivity Study

M. A. A. Salman,* and Mostafa S.A. ElSayed†
Carleton University, Ottawa, ON, K1S 5B6, Canada

Denis Walch‡
Bombardier Aerospace, St-Laurent, QC, H4S 1Y9, Canada

In this paper, the sensitivity of nonlinear dynamic aeroelastic loads of very flexible airframes to variations in multiple aircraft conceptual design parameters is investigated. It is found that the design changes with the largest effect on wings nonlinear loadings are those associated with variations in the wing out of plane stiffness as well as the geometrical variations associated with the Outer Mold Line modifications resulting in changes in the position of aerodynamic center. Changes of up to +5.2% and -4.8% in wings peak bending moments due to gust turbulences are found when geometric nonlinearities are considered in the aeroelastic loads analyses as compared to results of linear aeroelasticity simulations. Additionally, unlike most conceptual design variables investigated, it is found that changes in stiffness distribution renders a nonlinear load variation that cannot be estimated with a linear gradient based method.

I. Introduction

The development of high fidelity aircraft loads is a critical step in the design process of airframes. A major set of these loads are derived simulating aircraft in flight employing linearized structural modeling approaches adopted by several commercially available codes such as MSC Nastran [1]. While linear finite element models are appropriate for the modelling of most legacy aircraft due to their relatively stiff airframe designs, this is not the case in modern aircraft that are developed with a primary objective of weight minimization. Here, the use of structural solvers capable of accurately modeling nonlinearities become a necessity to derive high fidelity aircraft loads when the aircraft design space is fully explored.

The effects of geometrical nonlinearities on the aeroelastic loads of aircraft in static flight conditions has been studied thoroughly in the literature [2]–[5]. Displacement based geometrically nonlinear beam models have been used by Drela and incorporated in ASWING software [6], to model nonlinear behavior of airframes. Using a mixed formulation beam models, the nonlinear flutter performance of aircraft has been investigated by Patil et al [7], and Tang [8]. Ribiero [4] used the strain based beam model, developed originally by Brown and Shearer [9], [10], to create a fully nonlinear aeroelastic solver, namely, AeroFlex. More recently, Castellani et al. [3] used MSC Nastran [1] to create an ad-hoc nonlinear static aeroelastic solver [2], [3], which was later improved upon in the literature [11].

* Graduate Student, Department of Mechanical and Aerospace Engineering, Carleton University, ON, Canada
† Professor of Aerospace Engineering, Department of Mechanical and Aerospace Engineering, Carleton University, ON, Canada, AIAA Member.
‡ Engineering Specialist, Bombardier Aerospace, St Laurent, Qc, Canada

Some studies into the relationship between aircraft design parameters and corresponding performance have been performed in the past [11]–[13]. For example, Mardanpour et al. investigated the effect of engine position on flutter behavior and gust alleviation using nonlinear aeroelastic solvers [12], [13]. On the other hand, the effects of stiffness distribution on static aeroelastic loads have also been extensively studied [11]. It is found that the response of flexible airframes under dynamic loading conditions, such as gust turbulences, taking into consideration effects of geometrical nonlinearities is not as well studied in the literature. In this paper, we aim to provide readers with an insight into the effects of airframe conceptual design parameters on the nonlinear dynamic aeroelastic loads. We also discuss strategies of conservative dynamic loads estimation due to different conceptual design derivatives.

The paper is organized in four sections, after this introduction, the formulation of the gust model, and the methodology used for the sensitivity analyses are presented in section two. Section three includes the results of the sensitivity analyses and the significance of the different conceptual aircraft design parameters on the nonlinear aeroelastic loads are discussed. The paper is concluded in section four.

II. Theoretical Framework

This section outlines the methodology developed to investigate the effects of aircraft conceptual design parameters on aircraft aeroelastic loading. Here, wing root bending moment, as an integral value of the total wing bending distribution, is used as the representative load where we studied its sensitivity to variations of selected aircraft conceptual design parameters. MSC Nastran [1] and ASWING [6] software are bench marked against in-house developed code and are, respectively, used for linear aeroelastic and nonlinear aeroelastic analyses.

A. Sensitivity Analysis

Sensitivity of the wing root load, namely the out of plane bending moment, to a number of aircraft conceptual design parameters, shown in Table 1, is investigated. The design parameters are varied with respect to a baseline aircraft structure, and the corresponding linear and nonlinear loads are calculated.

Sensitivity of aeroelastic loads to variation in independent design parameter is determined with respect to the local derivative of the output using finite difference. This can be calculated as:

$$\zeta|_{\mathbf{\Delta_0}} = \left.\frac{\partial \Delta_e}{\partial \mathbf{\Delta}}\right|_{\mathbf{\Delta_0}} \tag{1}$$

where ζ is the local sensitivity, Δ_e is the increment in loads due to the effect of geometric nonlinearity, $\mathbf{\Delta}$ is the configuration of an arbitrary structural parameter at the current state, and $\mathbf{\Delta_0}$ is the value of the parameter in the aircraft structure's baseline configuration.

To evaluate Equation 1 and determine the sensitivity of a system with respect to a given configuration, the local derivative of the nonlinear increment is calculated numerically using either a backward-difference or central-difference gradient operator, depending on the design space of the parameter of interest [14].

B. Mass and stiffness variation

To vary the stiffness of the wing beam elements, each element is parameterized into a thin-walled rectangular box, as shown Figure 1, where a primary assumption is that the thickness of the wall is much less than the other dimensions.

The height of the thin-walled box is then varied from 50% to 100% of the baseline value. The resulting new box dimensions are used to recalculate the wing element structural properties.

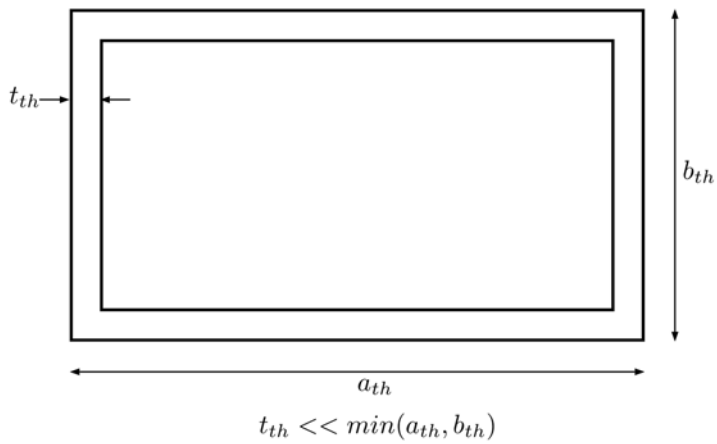

Figure 1: Dimensioning of thin-walled beam used to parameterize wing elements

The cross-sectional area, A, of the beam is simply calculated as:

$$A = 2t_{th}(a_{th} + b_{th}) \tag{2}$$

and the out-of-plane, in-plane, and polar moments of area are given as:

$$I_{11} = \frac{a_{th}t_{th}b_{th}^2}{3} \tag{3}$$

$$I_{22} = \frac{a_{th}^2 t_{th}b_{th}}{3} \tag{4}$$

$$J = \frac{2t_{th}^2(a_{th} - t_{th})^2(b_{th} - t_{th})^2}{b_{th}t_{th} + a_{th}t_{th} - 2t_{th}^2} \tag{5}$$

where a_{th} is the width of the beam, $b_{th}$is its height and t_{th} is the thickness of its wall. I_{11} and I_{22} are the second moments of area, and J is the polar moment of area. The th subscript is used due to the thin-walled beam assumption.

As the length of the beam element is fixed, its mass is calculated proportionally to the beam cross section area as:

$$M_{new} = \frac{A_{new}}{A_{base}} M_{base} \tag{6}$$

where the baseline elemental mass and cross-sectional area are represented by the subscript "$base$" and the modified parameters by "new".

The resulting mass and stiffness distributions are shown in Figure 2 where the normalized stiffness and mass values are expressed as function in the out-of-plane stiffness of the wing.

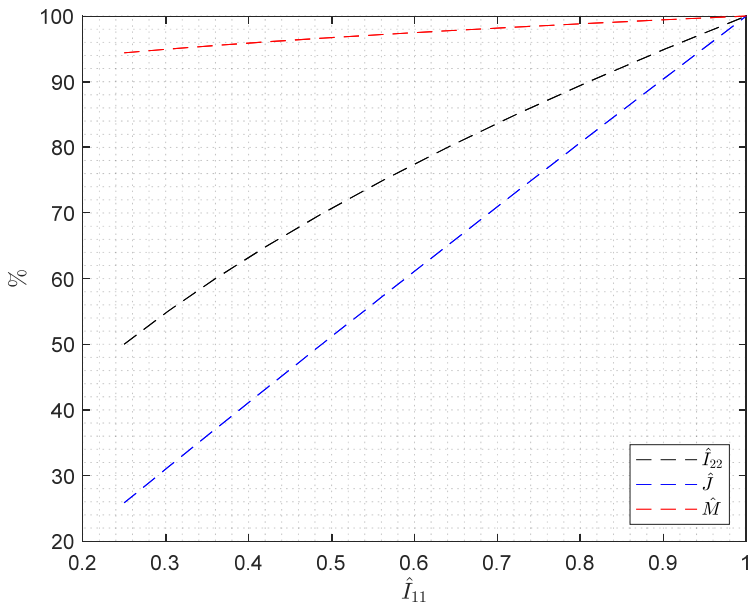

Figure 2: Variation of the in-plane stiffness, torsional stiffness, and element mass, as a function of out of plane stiffness

C. Stick model generation

For the purposes of this case study, a stick model of a Bombardier Aircraft platform is used, as a 3D Global Finite Element (GFEM) model would be computationally expensive to run. Several methods of airframe model order reduction are available in the literature [15]–[19]. In this paper, the unitary loading method is employed for the development of the airframe condensed stick model [19], [20].

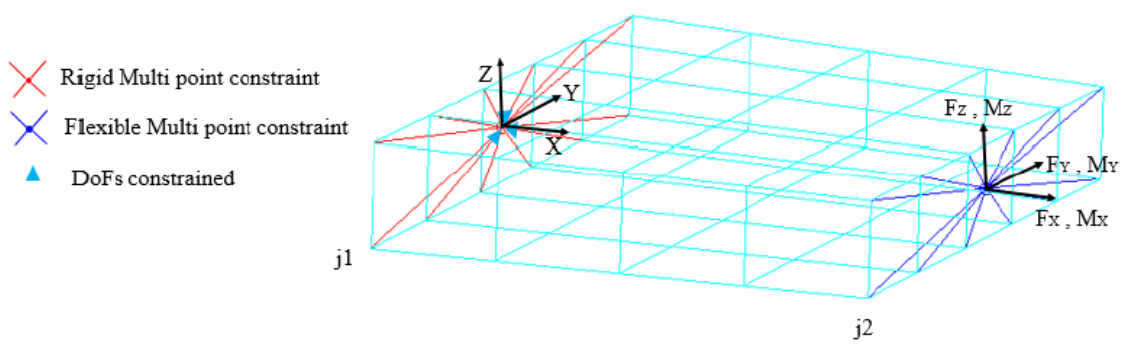

Figure 3: Schematic drawing showing GFEM reduction process to Stick Model

Figure 3 shows a schematic drawing that illustrates the stiffness extraction process of the stick model of a single bay of the 3D GFEM of aircraft wing box. For a given section, a cantilevered boundary condition is assumed with the inboard end, $j1$, is fixed. Six load cases involving unit forces and moments are applied

at the shear center of the free end, $j2$, and the stiffness properties for the beam element representing the wing bay are computed as:

$$A_{j1\to j2} = \frac{L_{j1\to j2}}{E\left|\delta_{j1\to j2}\right|_x} \tag{7}$$

where $A_{j1\to j2}$ is the equivalent cross-sectional area, $L_{j1\to j2}$ is the bay length, $\left|\delta_{j1\to j2}\right|_x$ is the axial elongation due to an applied unit load along the x axis, and E is the material Young's Modulus.

Similarly, the shear factors along the y and z directions, K_y and K_z respectively, are computed as:

$$\left(\mathrm{K}_y\right)_{j1\to j2} = \frac{L_{j1\to j2}}{GA_{j1\to j2}\left|\delta_{j1\to j2}\right|_y} \tag{8}$$

$$\left(\mathrm{K}_z\right)_{j1\to j2} = \frac{L_{j1\to j2}}{GA_{j1\to j2}\left|\delta_{j1\to j2}\right|_z} \tag{9}$$

where $\left|\delta_{j1\to j2}\right|_y$ and $\left|\delta_{j1\to j2}\right|_z$ are the translational deformation in the y and z directions due to a corresponding unit shear loading, and G is the shear modulus.

Moments of inertia of the stick model beam element are computed using the rotational deformations corresponding to the application of unit moments in the same manner as described before. The equivalent bending moments of inertia, I_y and I_z, along the y and z directions, as well as the torsional moment of inertia, J_x, in the x direction are given as:

$$\left(I_y\right)_{j1\to j2} = \frac{L_{j1\to j2}}{E\left|\theta_{j1\to j2}\right|_y} \tag{10}$$

$$\left(I_z\right)_{j1\to j2} = \frac{L_{j1\to j2}}{E\left|\theta_{j1\to j2}\right|_z} \tag{11}$$

$$\left(J_x\right)_{j1\to j2} = \frac{L_{j1\to j2}}{G\left|\theta_{j1\to j2}\right|_x} \tag{12}$$

where $\left|\theta_{j1\to j2}\right|_x$, $\left|\theta_{j1\to j2}\right|_y$, and $\left|\theta_{j1\to j2}\right|_z$ are the angular deformations along x, y, z directions due to a corresponding unit moment.

It should be noted that the standard practice in the aerospace industry for aeroelasticity analysis involves the use of lumped mass idealization of the 3D GFEM [19]. The equivalent lumped mass [21] for each aircraft bay can be easily calculated from the aircraft CAD model.

D. ASWING beam model

The nonlinear aeroelastic software employed for this work, ASWING, uses the Minguet nonlinear beam model [22]. ASWING is chosen due to its displacement-based beam formulation, as well as the fact that a previous study conducted by the author validates the results of ASWING for nonlinear aeroelastic loads [11]. The equations of motion are reproduced below.

Given a one-dimensional beam with warping effects ignored, the position along the beam can be represented as a single coordinate along the beam length, s. For any point along the beam, the relationship between the beam local undeformed frame $\boldsymbol{b}$ and global reference frame $\boldsymbol{A}$ is given as

$$\mathbf{p}_b = \underline{C^{bA}} \cdot \mathbf{p}_A \tag{13}$$

where $\mathbf{p}$ is a vector representing the bases for the corresponding frames of reference, and $\underline{C^{bA}}$ is the transformation matrix from the global to the local frame, given in terms of Euler angles.

Assuming the beam has arbitrary curvature and twist, moving an infinitesimal distance, ds, along the beam reference line rotates the local reference frame as follows:

$$\frac{d\underline{C^{bA}}}{ds} = [\boldsymbol{\kappa}]\underline{C^{bA}} \tag{14}$$

where the curvature matrix is given by:

$$[\boldsymbol{\kappa}] = \begin{bmatrix} 0 & \kappa_z & -\kappa_y \\ -\kappa_z & 0 & \kappa_x \\ \kappa_y & -\kappa_x & 0 \end{bmatrix} \tag{15}$$

and $\kappa_x, \kappa_y, \kappa_z$ are the curvatures of the beam about the beam axes.

The transformation matrix is given by pre-multiplication of the 3 individual rotations from the global to the local reference frame as:

$$\underline{C^{bA}} = \begin{bmatrix} 1 & 0 & 0 \\ 0 & \cos\theta_1 & \sin\theta_1 \\ 0 & -\sin\theta_1 & \cos\theta_1 \end{bmatrix} \begin{bmatrix} \cos\theta_2 & 0 & \sin\theta_2 \\ 0 & 1 & 0 \\ -\sin\theta_2 & 0 & \cos\theta_2 \end{bmatrix} \begin{bmatrix} \cos\theta_3 & \sin\theta_3 & 0 \\ -\sin\theta_3 & \cos\theta_3 & 0 \\ 0 & 0 & 1 \end{bmatrix} \tag{16}$$

Solving for the curvatures in Equation 15, the following expressions are obtained for the curvatures in terms of the Euler angles:

$$\tag{17}$$

$$\kappa_z = \sin\theta_1 \frac{d\theta_2}{ds} + \cos\theta_1 \cos\theta_2 \frac{d\theta_3}{ds}$$

The equations of motion for a differential beam element are then derived by solving for the equilibrium of a beam element in the deformed position. The beam internal stresses are defined by the local beam force, F_{int}, and moment, M_{int}, vectors.

The force equilibrium equation is given as:

$$\left[\underline{C^{bA}} + d\underline{C^{bA}}\right]^{\mathrm{T}}(\mathrm{F}_{int} + d\mathrm{F}_{int}) - \left[\underline{C^{bA}}\right]^{\mathrm{T}}\mathrm{F}_{int} + \left[\underline{C^{bA}}\right]^{\mathrm{T}}\mathrm{F}_b ds + \mathrm{F}_A ds = 0 \tag{18}$$

and the corresponding elemental moment equation is given as:

$$\begin{aligned}\left[\underline{C^{bA}} + d\underline{C^{bA}}\right]^{\mathrm{T}}(\mathrm{M}_{int} + d\mathrm{M}_{int}) - \left[\underline{C^{bA}}\right]^{\mathrm{T}}\mathrm{M}_{int} + \left[\underline{C^{bA}}\right]^{\mathrm{T}}\left(e_1 \times (\mathrm{F}_{int} + d\mathrm{F}_{int})\right) \\ + \left[\underline{C^{bA}}\right]^{\mathrm{T}}\mathrm{M}_b ds + \mathrm{M}_A ds = 0\end{aligned} \tag{19}$$

where F_b and M_b are, respectively, the external force and moment vectors applied in the beam local reference frame, such as aerodynamic loads, while F_A and M_A are, respectively, the applied loads in the global reference frame. e_1 is a vector tangent to the differential beam element where $e_1 = [ds, 0,0]^{\mathrm{T}}$.

The strain-displacement relations are then obtained by inverting Equations 17 to obtain the following relations relating rotations to curvatures:

$$\begin{aligned}\frac{d\theta_1}{ds} &= \kappa_x - \sin\theta_1 \tan\theta_2\, \kappa_y - \cos\theta_1 \tan\theta_2\, \kappa_z \\ \frac{d\theta_2}{ds} &= -\cos\theta_1\, \kappa_y + \sin\theta_1\, \kappa_z \\ \frac{d\theta_3}{ds} &= \frac{\sin\theta_1}{\cos\theta_2}\kappa_y + \frac{\cos\theta_1}{\cos\theta_2}\kappa_z\end{aligned} \tag{20}$$

The translation analogues are given as:

$$\begin{aligned}\frac{dx}{ds} &= (1+\varepsilon)\cos\theta_2 \cos\theta_3 \\ \frac{dy}{ds} &= (1+\varepsilon)\cos\theta_2 \sin\theta_3 \\ \frac{dz}{ds} &= (1+\varepsilon)\sin\theta_2\end{aligned} \tag{21}$$

where ε is the extensional strain along the beam, and x, y, z are the deformed beam coordinates.

The final relationships are the stress-strain relations which are given by the classical linear relationships as follows:

$$\begin{Bmatrix} \mathrm{F} \\ \mathrm{M} \end{Bmatrix} = S \begin{Bmatrix} \gamma \\ \kappa \end{Bmatrix} \tag{22}$$

where S is the sectional stiffness matrix, γ are the extensional and transverse strains, and κ are the curvatures.

In the absence of materials with coupling behaviours such as composites, the sectional stiffness matrix can be simply given as

$$S = \begin{bmatrix} EA & 0 & 0 & 0 & 0 & 0 \\ 0 & G\mathrm{K}_2 & 0 & 0 & 0 & 0 \\ 0 & 0 & G\mathrm{K}_3 & 0 & 0 & 0 \\ 0 & 0 & 0 & G\mathrm{J} & 0 & 0 \\ 0 & 0 & 0 & 0 & EI_2 & 0 \\ 0 & 0 & 0 & 0 & 0 & EI_3 \end{bmatrix} \tag{23}$$

where $G\mathrm{K}_2$ and $G\mathrm{K}_3$ are the shear stiffness, EI_2 and EI_3 are the bending stiffness, and EA and $G\mathrm{J}$ are the extensional and torsional stiffness, respectively.

Equations 18-22**Error! Reference source not found.** form a system of 12 nonlinear first order differential equations, which can be solved simultaneously using a finite difference method [22].

E. Aeroelastic model

In a standard aeroelastic analysis, the aerodynamic pressure, $\hat{f}_{aero}$, is related to the downwash, $\widehat{w}$, at the aerodynamic surfaces as:

$$\hat{f}_{aero} = \mathrm{q}_{\mathrm{dyn}} \mathbf{A}_{\mathrm{AIC}}^{-1} \widehat{w} \tag{24}$$

where $\mathrm{q}_{\mathrm{dyn}}$ is the dynamic pressure of the flight condition, and the Aerodynamic Influence Coefficient (AIC) matrix relates the downwash to the aerodynamic pressure.

The downwash is given as:

$$\widehat{w} = \mathbf{D}\mathbf{U}_{aero} + \widehat{w}^{g} \tag{25}$$

The Aerodynamic Influence Coefficient (AIC) matrix is given by $\mathbf{A}_{\mathrm{AIC}}$ and $\mathbf{D}$ is the matrix relating the displacements of the aerodynamic panels, $\mathbf{U}_{aero}$, to the downwash.

The total aerodynamic force vector of the structure, $\hat{L}$, can then be given as:

$$\hat{L} = \mathbf{S}\hat{f}_{aero} + \mathbf{F}_{rig} \tag{26}$$

where $\mathbf{S}$ is a matrix relating nodal pressures to nodal forces, and $\mathbf{F}_{rig}$ is a vector of rigid applied loads on the structure, such as engine loads and point loads.

The force-displacement relationship for a static structure is given by:

$$\mathbf{R} = \mathbf{K}_{\text{glob}}\mathbf{U} \tag{27}$$

where $\mathbf{R}$ is the total load on the structure, $\mathbf{U}$ is the global displacement vector due to the applied load, and $\mathbf{K}_{\text{glob}}$ is the global tangent stiffness matrix of the structure.

Equating the RHS of Equations 26 and 27, the expression for an aeroelastic system at equilibrium is given as:

$$\mathbf{S}\hat{f}_{aero} + \mathbf{F}_{rig} = \mathbf{K}_{\text{glob}}\mathbf{U} \tag{28}$$

Substituting Equations 24 and 25 into the above expression yield the following relationship

$$\underbrace{\mathrm{q}\mathbf{S}\mathbf{A}_{\text{AIC}}^{-1}}_{\mathbf{Q}}\left[\mathbf{D}\mathbf{U} + \widehat{w}^{g}\right] + \mathbf{F}_{rig} = \mathbf{K}_{\text{glob}}\mathbf{U} \tag{29}$$

MSC Nastran [1] is used for the linear aeroelastic analysis. Here, the dynamic aeroelastic equation of motion is given as:

$$\left[-\mathbf{M}_m\omega^2 + i\mathbf{C}_m\omega + \mathbf{K}_m - \mathrm{q}_{\text{dyn}}\mathbf{Q}_m\right]\mathbf{X}_m = \mathbf{R}(\omega) \tag{30}$$

where $\mathbf{M}_m, \mathbf{C}_m$ and $\mathbf{K}_m$ are the modal mass, damping and stiffness matrices, respectively, $\mathbf{Q}_m$ is a matrix relating the nodal downwash to the corresponding modal forces at the nodes, and $\mathbf{X}_m$ is a vector of generalized modal coordinates. ω is the frequency around which the system is reduced, and i is a complex number.

Equation 30 is solved with respect to an equilibrium condition, which in this work is taken to be a 1G steady flight condition. The physical solution is then obtained by taking the inverse Fourier Transform of the modal response, as follows:

$$\mathbf{U}(t) = \int_{-\infty}^{\infty} \mathbf{H}(\omega)\mathbf{R}(\omega)e^{i\omega t}\, d\omega \tag{31}$$

Where the transfer function $\mathbf{H}(\omega)$ is given as:

$$\mathbf{H}(\omega) = \frac{1}{\left[-\mathbf{M}_m\omega^2 + i\mathbf{C}_m\omega + \mathbf{K}_m - \mathrm{q}_{\text{dyn}}\mathbf{Q}_m\right]} \tag{32}$$

F. Aerodynamic model

Both ASWING and MSC Nastran use panel method aerodynamics to calculate the aerodynamic loads exerted on the aircraft structure [6], namely the Doublet Lattice Method [1], [23], [24]. This method is based on linearized potential flow theory, where a line of potential doublets of unknown strength lie along the quarter-chord of each aerodynamic panel. Given n aerodynamic boxes with a constant force per unit length along the quarter-chord line, $\mathbf{f}$, the strength of a doublet line segment j is given as

$$\frac{\mathbf{f}_j}{4\pi\rho_{air}} \int L_j \, ds \tag{33}$$

Where L_j is the length of the doublet line, ds is an increment along the line, and ρ_{air} is the density of air. The total downwash at any point on the aerodynamic surface (x_i, s_i) can then be written as the sum of all the downwash due to all the doublets on the surface.

$$\overline{w}(x_i, s_i) = \sum_{j=1}^{n} \left(\frac{\mathbf{f}_j}{4\pi\rho_{air}} U_{free}^2 \right) \int \hat{\Gamma} \, ds \tag{34}$$

Where U_{free} is the freestream velocity of the airflow across the panels, and $\hat{\Gamma}$ is the kernel function for a nonplanar surface [25].

When Equation 34 is applied to all the downwash points, the force per unit length along the quarter-chords of the boxes can be determined, and thus, the average pressure, f_{box}, on each aerodynamic box is written as:

$$f_{box_i} = \frac{\mathbf{f}_i}{\Delta x_j \, cos \, \lambda_j} \tag{35}$$

Where Δx_j is the average chord of the jth box, and λ_j is the sweep angle of the doublet line on the box. Given the jth index of doublet lines and ith index of the downwash points, Equation 34 can be re-written as:

$$\overline{w} = \sum_{j=1}^{n} D_{ij} p_j \tag{27}$$

where D_{ij} are the elements of matrix $\mathbf{D}$ in Equation 25, given as follows:

$$\frac{\pi}{8} \Delta x_j \cos \lambda_j \int \hat{\Gamma} \, ds \tag{36}$$

Equation 25 represents the downwash acting on an aerodynamic panel. However, trimming the aircraft into a steady state condition often requires the use of aerodynamic degrees of freedom, such as angle of attack, rotation rates, and control surface deflections, to modify the net forces and moments acting on the structure, which can be incorporated into the expression for the downwash as follows:

$$\hat{w} = \mathbf{DU} + \mathbf{D}_\sigma \hat{u}_\sigma + \hat{w}^g \tag{38}$$

where $\mathbf{D}_\sigma$ is a matrix relating the aerodynamic degrees of freedom, $\hat{u}_\sigma$, to the downwash. All prior equations assume that the aerodynamic forces are applied directly to the structural nodes. However, due to differences in the meshing of aerodynamic panels and structural members, this is not always the case. This is because the aerodynamic panels are applied at the quarter-chord point of each aerodynamic box element, which is

quite often much larger in number than the actual structural elements. The forces need to be coupled to the structural degrees of freedom of the airframe, which is achieved using a linear beam spline using an interpolation matrix.

$$\mathbf{U}_{aero} = \mathbf{G}_{\text{spline}}\mathbf{U}_{struct} \tag{39}$$

where $\mathbf{G}_{\text{spline}}$ is the interpolation matrix relating the structural deflections $\mathbf{U}_{struct}$, to the aerodynamic nodal deflections $\mathbf{U}_{aero}$

Imposing the condition that the virtual work performed by both deflections is identical, an expression for an arbitrary force transformation between the aerodynamic and structural nodes is given as follows

$$\mathbf{F}_{struct} = \left[\mathbf{G}_{\text{spline}}\right]^{\text{T}}\mathbf{F}_{aero} \tag{40}$$

where $\mathbf{F}_{aero}$ is a vector of aerodynamic loads on aerodynamic nodes, and $\mathbf{F}_{struct}$ are the resulting aerodynamic loads on structural nodes.

G. Discrete gust model

Discrete gust model is used in both the linear and nonlinear dynamic aeroelastic analyses. Unlike continuous disturbance models [26], in a discrete gust model, the disturbance is modeled as a single pulse of arbitrary shape and size. In this work, the 1 Minus Cosine (1MC) gust model is used as it more closely represents actual gust velocities in the atmosphere [27].

The vertical discrete gust velocity at a distance X into the gust profile is computed as:

$$U_{gust} = \frac{U_{ds}}{2}\left(1 - \cos\left(\frac{2\pi X}{L_{gust}}\right)\right) \tag{41}$$

where L_{gust} and U_{ds} are gust length and gust design velocity given by:

$$U_{ds} = U_{ref}g_g\left(\frac{0.5L_{gust}}{350}\right)^{\frac{1}{6}} \tag{42}$$

where U_{ref} is the reference gust velocity, and g_g is the flight profile alleviation factor.

However, it must be noted that the aerodynamic models used in ASWING and MSC Nastran are not identical, and as such, will have slightly differing lift distributions across the wingspan of the aircraft, especially during dynamic gust encounters.

III. Case Study

The following section presents the details of the model used for the case study, as well as details about the parameters used in the sensitivity analysis. For the purposes of this work, the gust design velocity, $U_{ds} = 78.9\ ft/s$, and the gust length, $L_{gust} = 100\ ft$ are considered.

A Bombardier Aircraft platform is used for the purposes of this study. The Global FE model is reduced to a stick model using the unitary loading method described in Section II. C. The stick model is originally

created in MSC. Nastran format, and then converted to ASWING format using an automated script for use with the geometrically nonlinear solver.

Table 1 gives the list of the parameters considered in this study, to determine their effect on the nonlinear moment increment, Δ_e, as well as the gradient operator used to compute the local sensitivity.

Table 1: Parameters being studied for the sensitivity analyses

$Parameter\ (\boldsymbol{\Delta})$[1]	$Baseline\ value\ (\boldsymbol{\Delta_0})$	$Lower\ limit$	$Upper\ limit$	Δ_{inc}	Finite difference type
$Out-of-plane\ stiffness\ (\hat{I}_{11})$	100%	25%	100%	7.5 %	Backward
$Wing\ position\ (\Delta_{W_{CA}})$	$0\ in$	$-5\ in$	$5\ in$	1 in	Central
$Tail\ position\ (\Delta_{T_{CA}})$	$0\ in$	$-10\ in$	$10\ in$	2 in	Central
$Engine\ position-longitudinal\ (\Delta_{E_{long}})$	$0\ in$	$-5\ in$	$5\ in$	1 in	Central
$Engine\ position-lateral\ (\Delta_{E_{lat}})$	$0\ in$	$-5\ in$	$5\ in$	1 in	Central
$Engine\ mass\ (\Delta_{E_M})$	0%	-5%	5%	1 %	Central

The hatted $\widehat{\ }$ notation represents values that are normalized with respect to the baseline aircraft's value.

A. Sensitivity due to change in wing stiffness distribution

To evaluate the sensitivity of the peak gust loads to the reduction in out of plane stiffness, $\hat{I}_{11}$, the backwards-difference gradient operator is used as:

$$\zeta|_{\boldsymbol{\Delta_0}} = \frac{\Delta_e(\boldsymbol{\Delta_0} - \Delta_{inc}) - \Delta_e(\boldsymbol{\Delta_0})}{\Delta_{inc}} \tag{43}$$

where Δ_{inc} is a small reduction in the out of plane wing stiffness with respect to the baseline aircraft value.

Here, the aircraft wing is assumed as a stick model [16] represented by a set of beam elements extending along the wing elastic axis.

B. Sensitivity by central difference method

The sensitivity of peak gust loads to the out of plane wing stiffness was presented separate from the other parameters due to the range of acceptable parameters used in this study. The rest of the parameters are varied with respect to their baseline conditions, $\boldsymbol{\Delta_0} = 0$, and as such, the local gradient can be calculated with the use of two points around the baseline value. As such, the gradient operator used to calculate the loads sensitivity to each individual parameter is the central difference method, given as:

[1] The delta notation, ($\boldsymbol{\Delta}$), represents small variations of a given parameter with respect to a baseline value of the original aircraft.

$$\zeta|_{\mathbf{\Delta_0}} = \frac{\Delta_e(\mathbf{\Delta_0} + \Delta_{inc}) - \Delta_e(\mathbf{\Delta_0} - \Delta_{inc})}{2\Delta_{inc}} \tag{44}$$

IV. Results and Discussions

The following section presents a comparison of the loads calculated by linear and nonlinear solvers and discusses the results of the parametric variation of the aircraft design parameters discussed in Section Theoretical FrameworkII.

A. Baseline comparison

To obtain a baseline comparison between the linear and the nonlinear dynamic aeroelastic solutions, a 1MC gust simulation is performed on the aircraft model to observe the time-domain behaviour of the aircraft between Nastran SOL 146 and ASWING. The resultant out of plane bending loads are shown in Figure 4. It can be observed that the primary peak bending loads occurring before $0.5s$ match closely between the two simulations. In this work, we are considering solely the effect of geometric nonlinearities on the primary peak loads, and as such, the ASWING model is deemed appropriate.

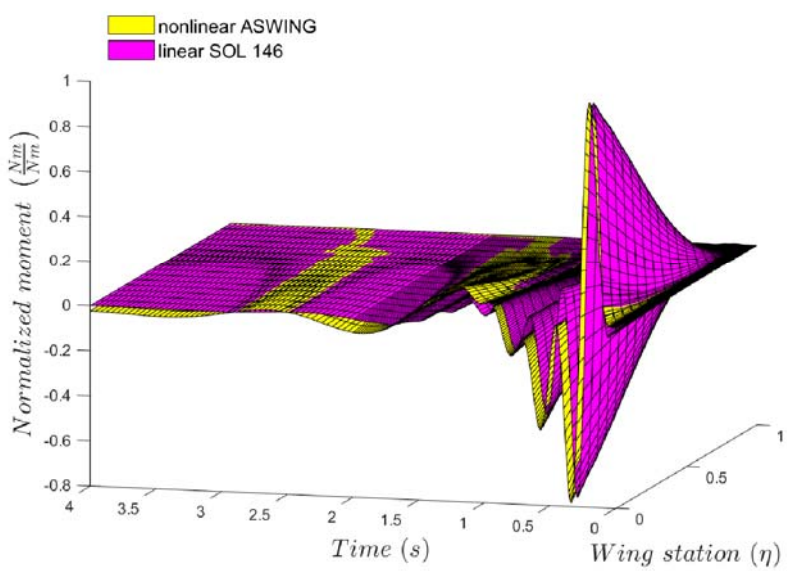

Figure 4: Normalized out of plane bending moment during dynamic gust simulation

B. Variation of Aircraft Design Parameters

For each design parameter, the results are shown for the maximum peak dynamic load using the nonlinear ASWING results, compared with the linear Nastran SOL146 results.

The results for the positive and negative peak bending moment, from both the linear SOL 146, and the nonlinear ASWING solvers are shown in Figure 5 and Figure 6 as a function of the varying out of plane stiffness, $\hat{I}_{11}$.

C. Variation of wing stiffness

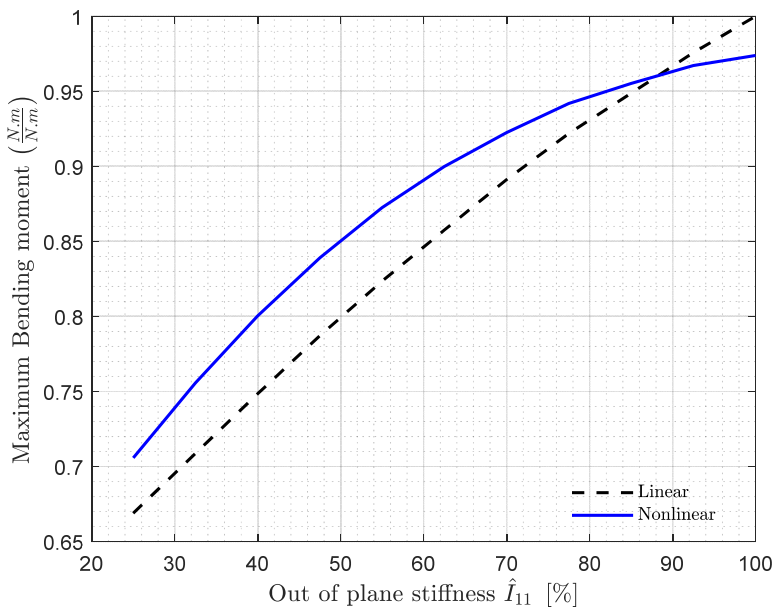

Figure 5: Variation in the positive peak gust load vs wing stiffness, $\hat{I}_{11}$

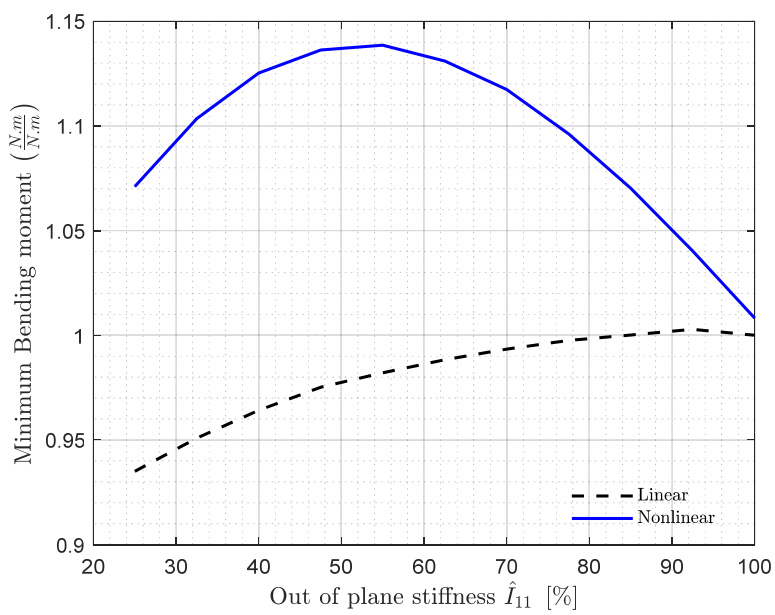

Figure 6: Variation in the negative peak gust load vs wing stiffness, $\hat{I}_{11}$

As shown in Figure 5 and Figure 6, the out of plane bending moments have a highly nonlinear relationship with respect to the reduction in wing stiffness. As the mass and stiffness of the wing reduce, the overall deflection of the wing increases, which leads to a higher root bending moment. This can be observed in the previous work by the author [11], where the nonlinear root bending moment due to the more flexible wings

are shown to be higher than the corresponding linear loads. However as this is a dynamic loading condition, there is another phenomenon in action, in which the highly deformable wing acts as a passive gust alleviation mechanism, reducing the peak loads on the structure [28]–[30].

D. Variation of wing-fuselage attachment point

In this study, the connection point between the elastic axes of the wing and fuselage is shifted about its default position on the baseline aircraft. Denoted ΔW_{CA}, this variation has the effect of changing the distance between the aircraft centre of gravity and the mean aerodynamic centre (MAC). Figure 7 provides a visual aid to understand the effect of varying ΔW_{CA}.

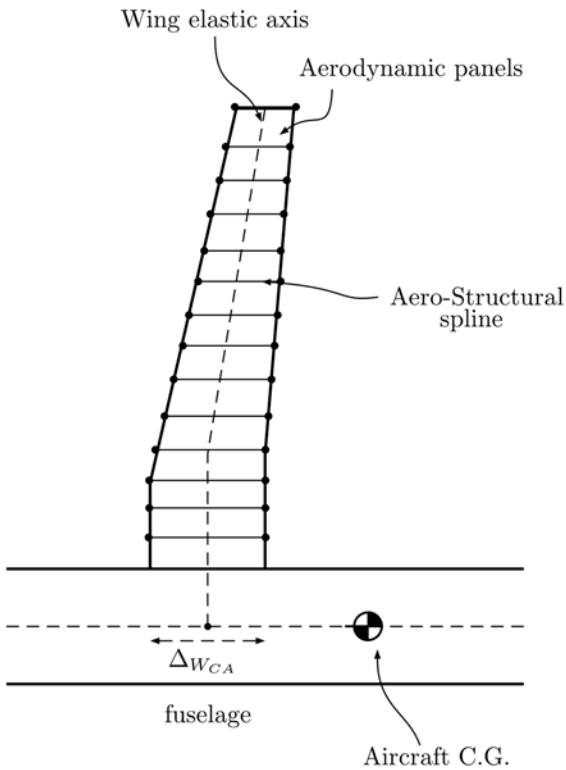

Figure 7: Wing-Fuselage attachment

The aerodynamic centre of the main wing was altered by shifting the attachment point between the wing and fuselage in the forward-aft direction, as shown in Figure 7.

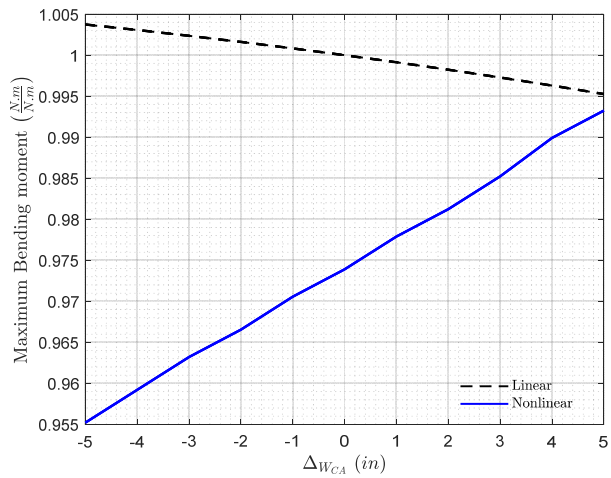

Figure 8: Variation in the positive peak gust load as the aerodynamic centre is moved forward and aft

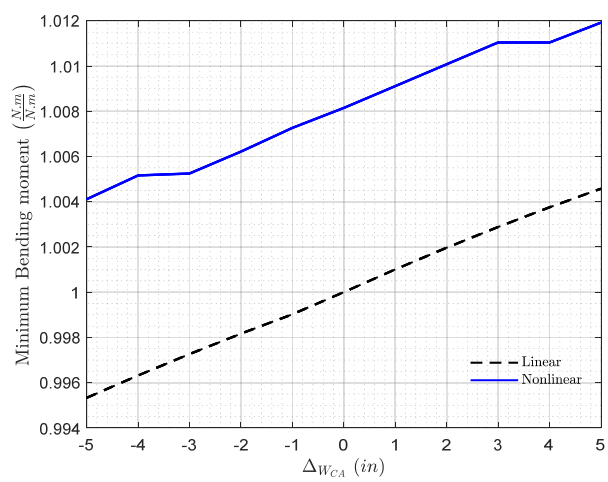

Figure 9: Variation in the negative peak gust load as the aerodynamic centre is moved forward and aft

The effect of these changes on the peak gust moments can be seen in Figure 8 and Figure 9. The changes in root bending loads are close to linear, since the shift in $\Delta_{W_{CA}}$ results in the linear increase or decrease of the proportion of the aircraft mass supported by the wing. The nonlinear positive peak loads vary by up to $\pm 2\%$ while the corresponding linear loads are varied by less than 0.5%. The change in the negative peak loads is less than 1% across the entire range of the design space.

E. Variation of tail elevator aerodynamic centre of pressure

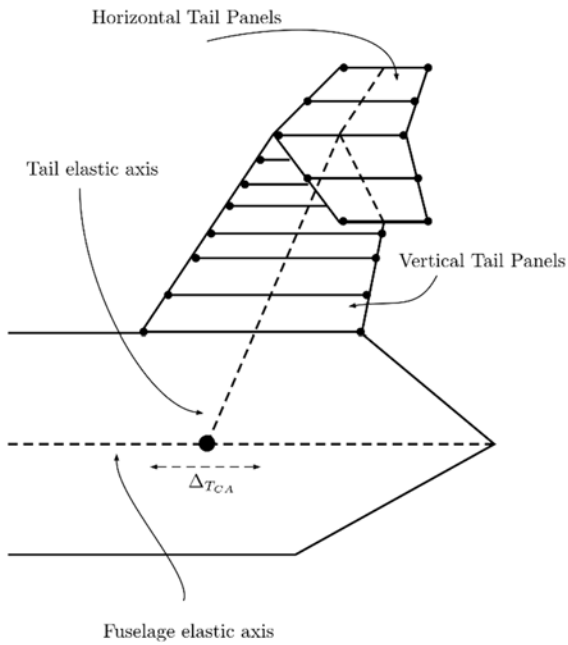

Figure 10: Tail-Fuselage attachment

Similarly to the shift in the wing aerodynamic centre, the attachment point of the tail assembly to the aircraft fuselage is shifted to study if there is any significant change in wing root bending moments.

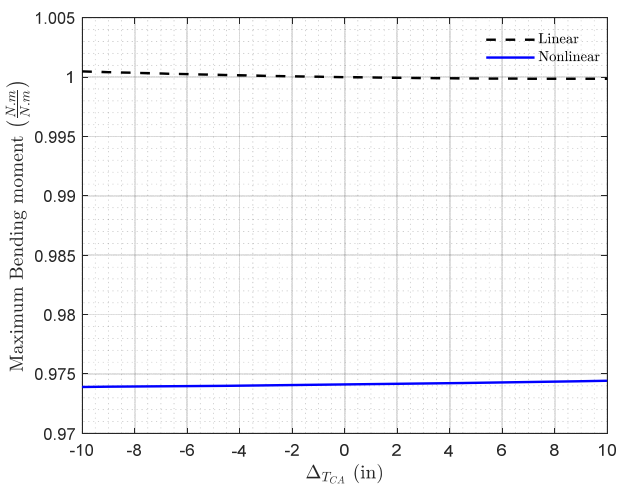

Figure 11: Variation in the positive peak gust load as the tail aerodynamic centre is moved forward and aft

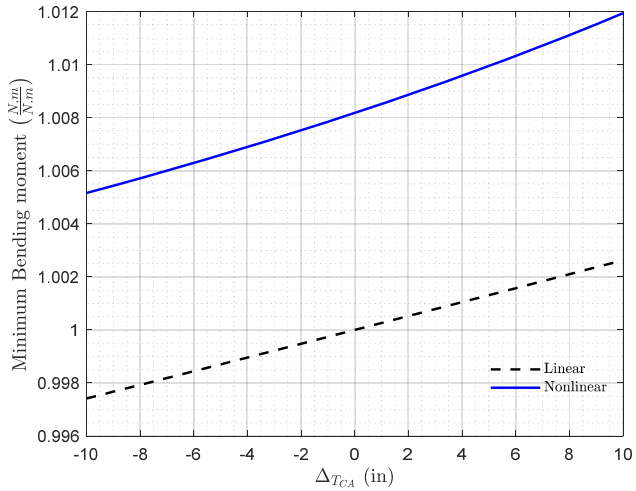

Figure 12: Variation in the negative peak gust load as the tail aerodynamic centre is moved forward and aft

Figure 11 and Figure 12 show that the variation in wing loads is negligible as the tail aerodynamic centre is shifted $\pm 5\ in$. This result is not unexpected as the shift in the overall centre of lift is not significantly affected by $\Delta_{T_{CA}}$ shift of a few inches.

F. Variation in engine longitudinal position

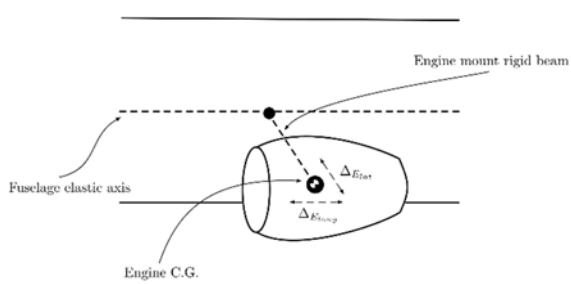

Figure 13: Engine C.G. shift

Figure 13 shows how the C.G. of the engine is shifted longitudinally along the fuselage and laterally perpendicular to it, to study the effects of engine positioning on nonlinear wing root moments.

The forward-aft position of the engine is shifted to observe the effects on the dynamic gust loads experienced, if any.

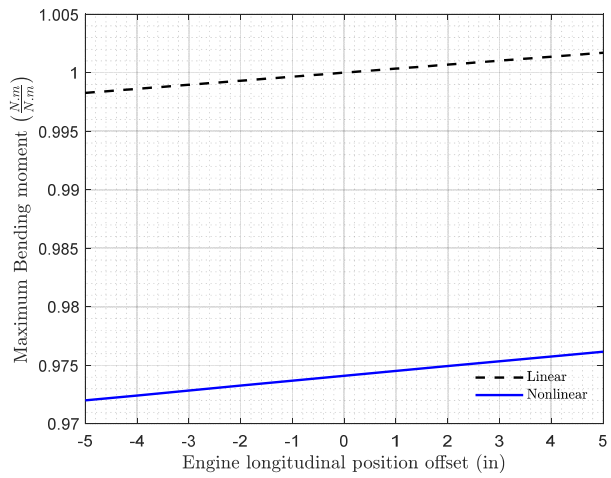

Figure 14: Variation in the positive peak gust load as the engine centre of mass is moved longitudinally

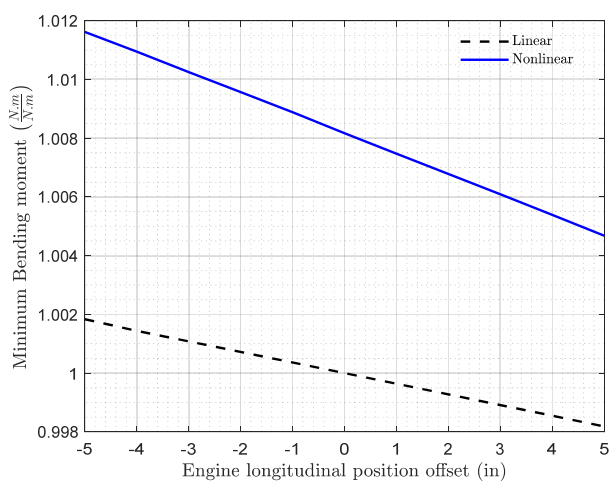

Figure 15: Variation in the negative peak gust load as the engine centre of mass is moved longitudinally

The shift in the engine longitudinal position results in overall loads changes of less than 1%, as the aircraft centre of gravity is shifted closer to the wing when $\Delta_{E_{long}}$ is negative.

G. Variation in engine lateral position

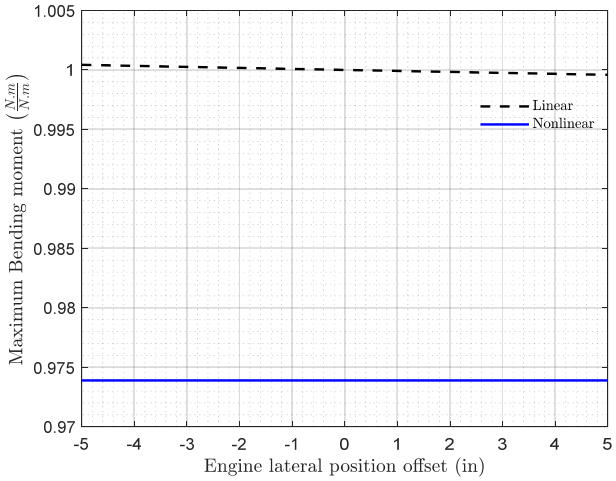

Figure 16: Variation in the positive peak gust load as the engine centre of mass is moved laterally

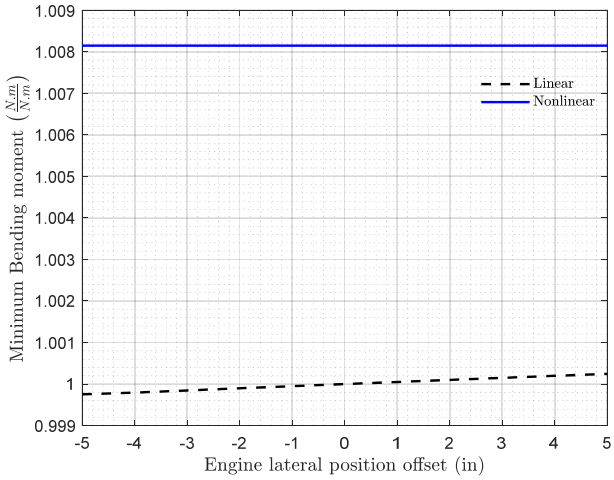

Figure 17: Variation in the negative peak gust load as the engine centre of mass is moved laterally

The change in loads due to lateral engine C.G. shifts, shown in Figure 16 and Figure 17, are negligible as they do not change the C.G. of the aircraft, thus keeping the overall load on the wing the same.

H. Variation in engine mass

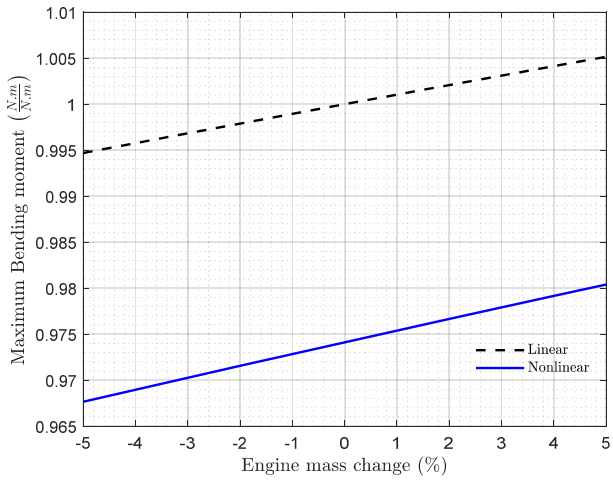

Figure 18: Variation in the positive peak gust load as the engine mass is varied by $\pm 5\%$

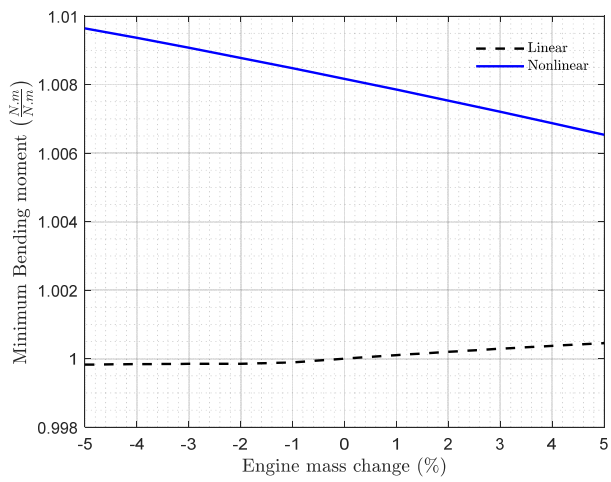

Figure 19: Variation in the negative peak gust load as the engine mass is varied by $\pm 5\%$

The positive peak loads increase with the increase to the engine mass, while the negative nonlinear peak loads can be seen to follow the opposite trend.

V. Sensitivity Analysis

In this section, the results from the previous section are studied to determine the baseline airframe's sensitivity to change in various structural parameters when geometrically nonlinear effects are considered. The maximum allowable error in dynamic loads, determined to be 0.8% for this specific aircraft platform, is denoted by the dashed red line.

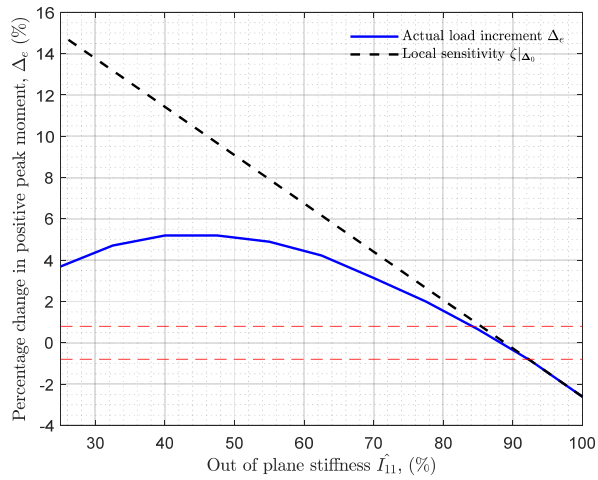

Figure 20: Sensitivity of nonlinear loads to variations in out of plane stiffness

The local sensitivity around the baseline stiffness of the aircraft, $\zeta|_{\mathbf{\Delta_0}}$, deviates significantly from the actual change in nonlinear bending moment, Δ_e, as calculated by the nonlinear solver. This is explained as the combined effect of passive gust load alleviation due to flexible wings [28]–[30] as well as increasing nonlinear loads due to large wing deflections [11]. As shown in Figure 20, the highly nonlinear behaviour cannot be estimated with a sensitivity analysis with respect to the baseline structure.

I. Changes in wing and tail aerodynamic centre

The positioning of the aerodynamic centre, $\Delta_{W_{CA}}$, is adjusted by shifting all aerodynamic and structural elements associated with the wing in the forward-aft direction.

The movement of the aerodynamic center along the fuselage changes the stability of aircraft. As the center of gravity is located behind the center of lift, moving the center of lift closer towards the center of gravity increases the value of the loads exerted by the wing. This can be seen in Figure 8 and Figure 9, where the normalized values of the root bending moment increase as the aerodynamic center is shifted closer to the aircraft's center of gravity.

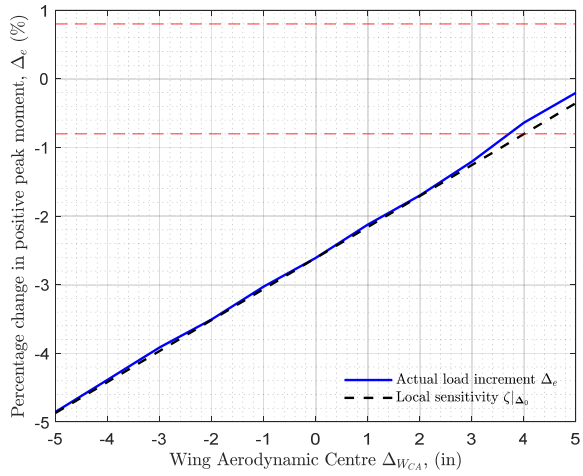

Figure 21: Sensitivity of nonlinear loads to variations in wing positioning

The sensitivity of the nonlinear load increment, Δ_e, to the shift in the positioning of the tail aerodynamic centre, $\Delta_{T_{CA}}$, is shown in Figure 22.

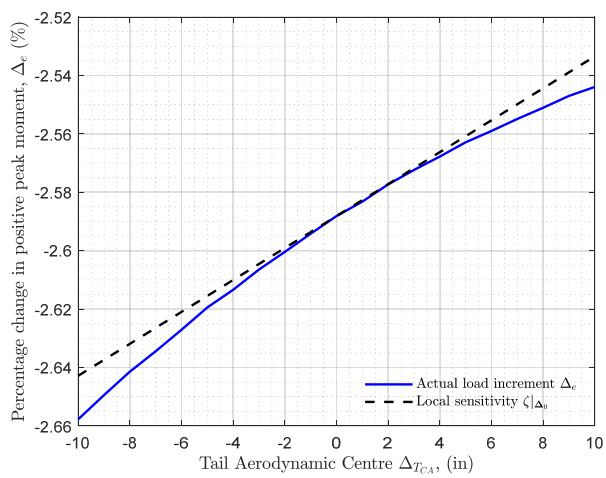

Figure 22: Sensitivity of nonlinear loads to variations in tail positioning

Unlike the shift in the aerodynamic centre of the wing, shifts in the position of the wing are not as significant to the nonlinear loads, with the overall load differences between the linear and nonlinear solution methods, Δ_e, of less than 1% over the entire design space. This is due to the fact that the magnitude of the loads on the aircraft wing do not shift much as a result of the shift in tail position, as seen in Figure 11 and Figure 12, where these changes result in less than 0.1% changes in the linear and nonlinear root bending moments at the wing.

J. Changes in engine mass and position

The changes in the engine mounting positions in the forward-aft and spanwise lateral directions, $\Delta_{E_{long}}$ and $\Delta_{E_{lat}}$ respectively, as well as the changes in the mass of the engine itself, Δ_{E_m}, are seen to have minimal impact on the nonlinear root bending moment of the aircraft wing. The sensitivity of the nonlinear loads, Δ_e, to these engine design parameters, are shown in Figure 23 - Figure 25, and contribute to less than 1% differences in the peak loads experienced by the aircraft wing root.

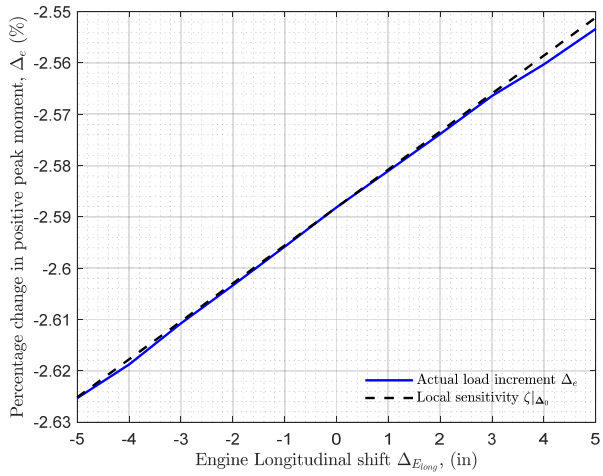

Figure 23: Sensitivity of nonlinear loads to variations in engine longitudinal position

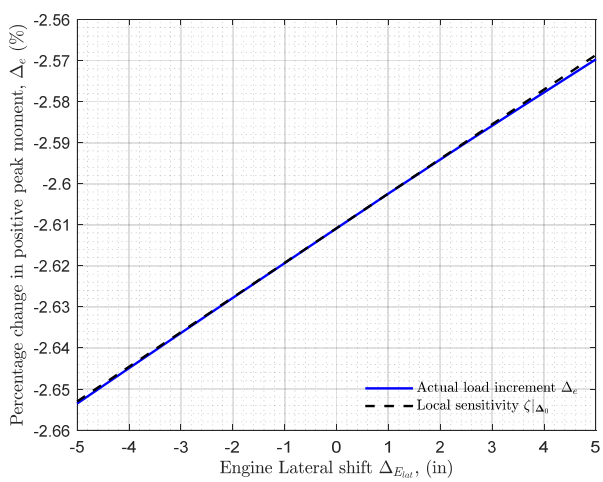

Figure 24: Sensitivity of nonlinear loads to variations in engine lateral position

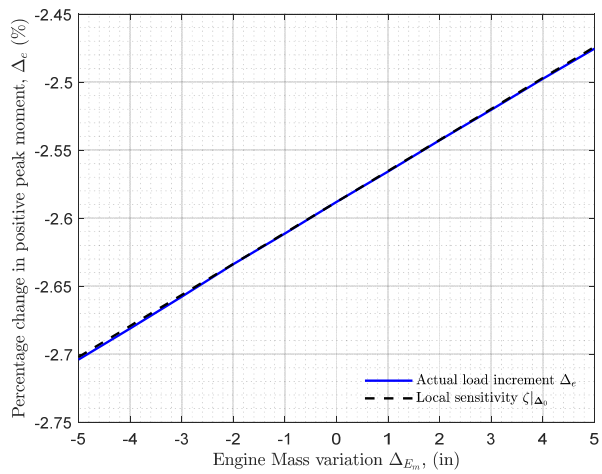

Figure 25: Sensitivity of nonlinear loads to variations in engine mass changes

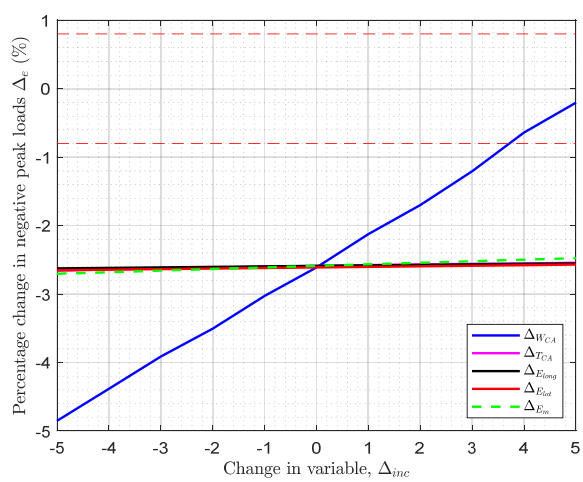

Figure 26: Sensitivity of nonlinear bending peak loads to variations of design parameters

VI. Conclusion

The results presented in this paper aim to help users at the early design stage of an aircraft determine if design choices need to be recalculated at every design iteration, or if they can be estimated based on a local-sensitivity based approach.

It is found that the only variable with significant changes to the loads between linear and nonlinear solvers are changes to the out of plane stiffness of the wing, where the change in load due to inclusion of geometrically nonlinear effects is highly nonlinear, and thus cannot be estimated based on local sensitivity. The changes to the tail-fuselage positioning, and engine mass and position variations are found to have an overall change of less than 1% across the design space, indicating a relative lack of influence on the nonlinearity of the results.

This indicates that for these parameters, a fully nonlinear design space computation is not necessary, as a sensitivity analysis of the gradient around the baseline configuration, $\zeta|_0$, matches with the actual loads difference, Δ_e, very well as can be seen in Figure 21, Figure 22, Figure 23, Figure 24, and Figure 25.

VII. Acknowledgements

The research presented in this paper is funded by Bombardier Aerospace, the Consortium for Aerospace Research and Innovation in Canada (CARIC) and by Mitacs Canada.

VIII. References

[1] W. P. Rodden and E. H. Johnson, *MSC/NASTRAN aeroelastic analysis: user's guide; Version 68*. MacNeal-Schwendler Corporation, 1994.

[2] M. Castellani, J. E. Cooper, and Y. Lemmens, "Nonlinear static aeroelasticity of high-aspect-ratio-wing aircraft by finite element and multibody methods," *J. Aircr.*, pp. 1–13, 2016.

[3] C. Howcroft *et al.*, "Aeroelastic modelling of highly flexible wings," in *15th Dynamics Specialists Conference*, 2016, p. 1798.

[4] F. Ribeiro, P. Paglione, R. G. A. da Silva, and M. S. de Sousa, "Aeroflex: a toolbox for studying the flight dynamics of highly flexible airplanes," in *Congresso Nacional de Engenharia Mecânica*, 2012, pp. 1786–2012.

[5] M. J. Patil, D. H. Hodges, and C. E. S. Cesnik, "Nonlinear aeroelasticity and flight dynamics of high-altitude long-endurance aircraft," *J. Aircr.*, vol. 38, no. 1, pp. 88–94, 2001.

[6] M. Drela, "ASWING 5.99 Technical Description," *Massachusetts Inst. Technol. Cambridge, MA*, 2015.

[7] M. J. Patil, D. H. Hodges, and C. E. S. Cesnik, "Characterizing the effects of geometrical nonlinearities on aeroelastic behavior of high-aspect ratio wings," in *Proceedings of the International Forum on Aeroelasticity and Structural Dynamics*, 1999, pp. 501–510.

[8] D. Tang and E. H. Dowell, "Experimental and theoretical study on aeroelastic response of high-aspect-ratio wings," *AIAA J.*, vol. 39, no. 8, pp. 1430–1441, 2001.

[9] E. L. Brown, "Integrated strain actuation in aircraft with highly flexible composite wings," 2003.

[10] C. M. Shearer, "Coupled Nonlinear Flight Dynamics, Aeroelasticity, and Control of Very Flexible Aircraft," 2006.

[11] M. A. A. Salman, M. S. A. ElSayed, and D. Walch, "Structural Nonlinearities and their Impact on the Fidelity of Critical Steady Maneuver Loads and Trimming Con figuration of Very Flexible Airframes," *J. Aeroelasticity Struct. Dyn.*, vol. 6, no. 1, 2018.

[12] P. Mardanpour, D. H. Hodges, R. Neuhart, and N. Graybeal, "Engine placement effect on nonlinear trim and stability of flying wing aircraft," *J. Aircr.*, vol. 50, no. 6, pp. 1716–1725, 2013.

[13] P. Mardanpour, E. Izadpanahi, S. Rastkar, and D. H. Hodges, "Nonlinear Aeroelastic Gust Suppression and Engine Placement," *J. Aircr.*, vol. 54, no. 6, pp. 2402–2404, 2017.

[14] K.-J. Bathe, *Finite Element Procedures*. Klaus-Jurgen Bathe.

[15] M. Hashemi-Kia and M. Toossi, "Development and application of a technique for reducing airframe finite element models for dynamics analysis," 1990.

[16] M. S. A. Elsayed, R. Sedaghati, and M. Abdo, "Accurate stick model development for static analysis of complex aircraft wing-box structures," *AIAA J.*, vol. 47, no. 9, pp. 2063–2075, 2009.

[17] G. Bindolino, G. Ghiringhelli, S. Ricci, and M. Terraneo, "Multilevel structural optimization for preliminary wing-box weight estimation," *J. Aircr.*, vol. 47, no. 2, pp. 475–489, 2010.

[18] R. CIRILLO, "Detailed and condensed finite element models for dynamic analysis of a business jet aircraft," 2011.

[19] G. Corriveau and F. Dervault, "Impact of Wing Box Geometrical Parameters on Stick Model Prediction Accuracy," in *54th AIAA/ASME/ASCE/AHS/ASC Structures, Structural Dynamics, and Materials Conference*, 2013, p. 1810.

[20] A. K. Singh and C. W. Nichols, "Derivation of an equivalent beam model from a structural finite element model," in *Proceedings of the MSC 1988 World Users Conference*, 1988.

[21] J. B. E. Bosco J. Morlier and A. Lucchetti, "Influence of mass modelling in dynamic landing simulations," in *10th PEGASUS-AIAA student conference*, 2014.

[22] P. J. Minguet, "Static and dynamic behavior of composite helicopter rotor blades under large deflections," Massachusetts Institute of Technology, 1989.

[23] E. Albano and W. P. Rodden, "A doublet-lattice method for calculating lift distributions on oscillating surfaces in subsonic flows.," *AIAA J.*, vol. 7, no. 2, pp. 279–285, 1969.

[24] W. P. Rodden, J. P. Giesing, and T. P. Kalman, "Refinement of the nonplanar aspects of the subsonic doublet-lattice lifting surface method.," *J. Aircr.*, vol. 9, no. 1, pp. 69–73, 1972.

[25] H. T. Vivian and L. V Andrew, "Unsteady aerodynamics for advanced configurations. part i. application of the subsonic kernel function to nonplanar lifting surfaces," 1965.

[26] J. K. Zbrozek, *The relationship between the discrete gust and power spectra presentations of atmospheric turbulence, with a suggested model of low-altitude turbulence*. HM Stationery Office, 1961.

[27] H. I. Flomenhoft, "Brief history of gust models for aircraft design," *J. Aircr.*, 1994.

[28] K. Fidkowski, I. Kroo, K. Willcox, and F. Engelson, "Stochastic Gust Analysis Techniques for Aircraft Conceptual Design," in *12th AIAA/ISSMO Multidisciplinary Analysis and Optimization Conference*, 2008.

[29] B. C. B. Tse, "Effects of Inertial and Geometric Nonlinearities in the Simulation of Flexible Aircraft Dynamics," University of Toronto, 2013.

[30] R. G. Cook, R. Palacios, and P. Goulart, "Robust Gust Alleviation and Stabilization of Very Flexible Aircraft," *AIAA J.*, 2013.